2011 50th IEEE Conference on Decision and Control and
European Control Conference (CDC-ECC)
Orlando, FL, USA, December 12-15, 2011

Computation of the frequency responses for distributed systems with one spatial variable

Binh K. Lieu and Mihailo R. Jovanović

Abstract— **For a class of distributed systems with one spatial variable, we develop a method for computing the maximum singular value of the frequency response operator. This computation is typically done by resorting to finite-dimensional approximations of the underlying operators. In this paper, we introduce an alternative approach that avoids the need for numerical approximation of the operators in the evolution model. This involves two steps: (i) recasting the frequency response operator as a two point boundary value problem; and (ii) using state-of-the-art automatic spectral collocation techniques for solving the resulting boundary value problems with accuracy comparable to machine precision. We provide an example from viscoelastic fluid dynamics to illustrate the utility of the proposed method.**

I. Introduction

We study the frequency responses of distributed systems in which an independent spatial variable belongs to a finite interval. In particular, we are interested in determining the maximum singular value of the frequency response operator and its corresponding left and right singular functions. Computation of frequency responses for this class of systems is typically done numerically using finite-dimensional approximations of the operators in the evolution model. For example, pseudo-spectral methods (PSMs) [1] represent a powerful tool for discretization of differential operators; they possess superior numerical accuracy compared to approximation schemes based on finite differences and they typically yield reliable results. However, there are two major difficulties that PSMs may encounter when dealing with systems that contain differential operators of high order. First, PSMs may produce unreliable results and even fail to converge upon grid refinement; this lack of convergence is attributed to the loss of accuracy due to ill-conditioning of the discretized differentiation matrices [2]. Second, boundary conditions satisfaction is one of the major difficulty in using these methods.

In this paper, we introduce a method that avoids the need for finite dimensional approximations of differential operators in the evolution model. This is accomplished by recasting the frequency response operator as a two point boundary value problem (TPBVP) that is given by either an input-output differential equation or by a corresponding spatial state-space representation. These transformations enable the use of recently developed computational tools, Chebfun [3] and bvp4c [4], that can solve boundary value problems with superior accuracy. Furthermore, boundary conditions can be easily implemented in the proposed setup. Chebfun is a collection of algorithms and software systems for numerical computations that involve functions and operators; Chebfun can handle problems that range from basic linear algebra to complex nonlinear boundary value problems. The major advantage of Chebfun is its ability to represent functions and operators using an automatic Chebyshev spectral collocation method; this feature eliminates the need for grid-point convergence test. On the other hand, bvp4c is a powerful numerical solver for systems of first order differential equations with boundary conditions. It implements a Simpson's method for computing the approximate solution to the two point boundary value problem. Similar to Chebfun, bvp4c also incorporates an adaptive mesh refinement technique that automatically determines the appropriate number of collocation points needed for accurate representation of the computed solution. Using an example from non-Newtonian fluid mechanics, which is notoriously difficult to handle numerically [5], [6], we illustrate the utility of our developments in producing results that exhibit much better accuracy than conventional finite dimensional approximation schemes.

Our presentation is organized as follows. In Section II, we formulate the problem and discuss the notion of a frequency response for distributed systems. In Section III, we present the method for converting the frequency response operator into a TPBVP that can be posed as an input-output differential equation or as a spatial space-space representation. In Section IV, we describe the numerical methods for computing the maximum singular value of the frequency response operator. In Section V, we demonstrate the utility of our developments by providing an example from viscoelastic fluid dynamics. We conclude with a summary of our developments in Section VI.

II. Problem formulation

We study the frequency responses of distributed systems with the evolution model

$$\partial_t \mathcal{E}\,\boldsymbol{\phi}(y,t) = \mathcal{F}\,\boldsymbol{\phi}(y,t) + \mathcal{G}\,\mathbf{d}(y,t), \tag{1a}$$

$$\boldsymbol{\varphi}(y,t) = \mathcal{H}\,\boldsymbol{\phi}(y,t), \tag{1b}$$

where $t \in [0,\infty)$ and $y \in [a,b]$ denote the temporal and spatial variables. The spatially distributed and time varying state, input, and output fields are represented by $\boldsymbol{\phi}$, $\mathbf{d}$, and $\boldsymbol{\varphi}$, respectively. At each t, $\mathbf{d}(\cdot,t)$ and $\boldsymbol{\varphi}(\cdot,t)$ denote the square-integrable vector-valued functions and $\mathcal{E}$, $\mathcal{F}$, $\mathcal{G}$, and $\mathcal{H}$ are matrices of differential operators with, in general, spatially varying coefficients. For example, the ijth entry

B. K. Lieu and M. R. Jovanović are with the Department of Electrical and Computer Engineering, University of Minnesota, Minneapolis, MN 55455, USA (e-mails: lieux006@umn.edu, mihailo@umn.edu).

Financial support from the National Science Foundation under CAREER Award CMMI-06-44793 is gratefully acknowledged.

of the operator $\mathcal{F}$ can be expressed as

$$\mathcal{F}_{ij} = \sum_{k=0}^{n_{ij}} f_{ij,k}(y) D^{(k)},$$

where each $f_{ij,k}$ is a smooth function on the interval $[a, b]$, $D^{(k)} = \partial^k / \partial y^k$, and n_{ij} is the highest differential order of $\mathcal{F}_{ij}$.

Application of the temporal Fourier transform yields the frequency response operator of system (1) [7], [8]

$$\mathcal{T}(\omega) = \mathcal{H} \left(\mathrm{j}\omega \mathcal{E} - \mathcal{F} \right)^{-1} \mathcal{G}, \tag{2}$$

where ω is the temporal frequency, and j is the imaginary unit. For an exponentially stable system (1), (2) describes the steady-state response to harmonic input signals across the frequency ω. Namely, if the input is harmonic in t, i.e., $\mathbf{d}(y,t) = \bar{\mathbf{d}}(y,\omega) \mathrm{e}^{\mathrm{j}\omega t}$, with $\bar{\mathbf{d}}(\cdot,\omega)$ denoting some spatial distribution in y, then the output is also harmonic in t with the same frequency but with a modified amplitude and phase

$$\boldsymbol{\varphi}(y,t) \;=\; \left(\left[\mathcal{T}(\omega) \bar{\mathbf{d}}(\omega) \right](y) \right) \mathrm{e}^{\mathrm{j}\omega t}.$$

Note that the amplitude and phase are precisely determined by the frequency response at the frequency ω.

The nth singular value of the frequency response operator $\mathcal{T}$ is determined by

$$\sigma_n^2 \left(\mathcal{T} \right) \;=\; \lambda_n \left(\mathcal{T} \mathcal{T}^* \right),$$

where $\lambda_n(\cdot)$ denotes the nth eigenvalue of a given operator and $\mathcal{T}^*$ represents the adjoint operator. For any fixed ω, the maximum singular value, $\sigma_{\max}(\mathcal{T}) = \max_n \sigma_n(\mathcal{T})$, determines the largest amplification from $\mathbf{d}$ to $\boldsymbol{\varphi}$ and it can be used to characterize the robustness of a system [9].

The computation of $\sigma_{\max}(\mathcal{T})$ is typically done numerically using finite dimensional approximations of the differential operators in (1). In this work, we develop alternative methods for computing $\sigma_{\max}(\mathcal{T})$. These methods do not require numerical approximation of the operators in (1). Instead, we reformulate the frequency response operator (2) into a TPBVP that can be solved with superior accuracy using recently developed computational tools. We illustrate the utility of our developments on an example from viscoelastic fluid dynamics, where finite dimensional approximation techniques fail to produce reliable results.

III. Two point boundary value representations of $\mathcal{T}$, $\mathcal{T}^*$, and $\mathcal{T}\mathcal{T}^*$

In this section, we first describe the procedure for determining the two point boundary value representations of the frequency response operator (2). These are given by either a high-order input-output differential equation or by a system of first-order differential equations in spatial variable y. We then discuss the procedure for obtaining corresponding representations of the adjoint operator $\mathcal{T}^*$ and the operator $\mathcal{T}\mathcal{T}^*$.

A. Representations of the frequency response operator $\mathcal{T}$

The temporal Fourier transform of (1) with zero initial conditions yields [7]

$$\left(\mathrm{j}\omega \mathcal{E} - \mathcal{F} \right) \boldsymbol{\phi}(y,\omega) \;=\; \mathcal{G}\, \mathbf{d}(y,\omega), \tag{3a}$$

$$\boldsymbol{\varphi}(y,\omega) \;=\; \mathcal{H}\, \boldsymbol{\phi}(y,\omega). \tag{3b}$$

System (3) represents a family of ordinary differential equations (ODEs), with boundary conditions at a and b, parameterized by the temporal frequency ω. Using the definitions of the operators in (3), we obtain the following differential equations

$$\mathcal{T} : \left\{ \begin{array}{rcl} \left[\mathcal{A}_0\, \boldsymbol{\phi} \right](y) & = & \left[\mathcal{B}_0\, \mathbf{d} \right](y), \\ \boldsymbol{\varphi}(y) & = & \left[\mathcal{C}_0\, \boldsymbol{\phi} \right](y), \\ 0 & = & \left[\mathcal{N}_0\, \boldsymbol{\phi} \right](y), \end{array} \right. \tag{4}$$

where

$$\begin{aligned} \mathcal{A}_0 \;&=\; \sum_{i=0}^{n} \boldsymbol{\alpha}_i(y)\, \mathbf{D}^{(i)}, \;\; \mathcal{B}_0 \;=\; \sum_{i=0}^{m} \boldsymbol{\beta}_i(y)\, \mathbf{D}^{(i)}, \\ \mathcal{C}_0 \;&=\; \sum_{i=0}^{k} \boldsymbol{\gamma}_i(y)\, \mathbf{D}^{(i)}, \\ \mathcal{N}_0 \;&=\; \sum_{i=0}^{\ell} \left(\mathbf{W}_{a,i}\, \mathbf{E}_a \;+\; \mathbf{W}_{b,i}\, \mathbf{E}_b \right) \mathbf{D}^{(i)}, \\ \mathbf{D}^{(i)} \;&=\; \begin{bmatrix} D^{(i)} & & \\ & \ddots & \\ & & D^{(i)} \end{bmatrix}, \;\; \boldsymbol{\phi} \;=\; \begin{bmatrix} \phi_1 \\ \vdots \\ \phi_s \end{bmatrix}. \end{aligned}$$

Here, $D^{(i)}\phi = \mathrm{d}^i\phi / \mathrm{d}y^i$, $\mathbf{E}_a$ and $\mathbf{E}_b$ denote the point evaluation functionals at the boundaries, e.g.,

$$\left[\mathbf{E}_a\, \boldsymbol{\phi} \right](y) \;=\; \boldsymbol{\phi}(a),$$

and $\{\mathbf{W}_{a,i},\ \mathbf{W}_{b,i}\}$ are constant matrices that specify the boundary conditions on $\boldsymbol{\phi}$. For notational convenience we have omitted the dependence on ω in (4), which is a convention that we adopt from now on. Here, n, m, k, and ℓ denote the highest differential orders of the operators $\mathcal{A}_0$, $\mathcal{B}_0$, $\mathcal{C}_0$, and $\mathcal{N}_0$, respectively. If the number of components in $\boldsymbol{\phi}$, $\mathbf{d}$, and $\boldsymbol{\varphi}$ is given by s, r, and p, then $\{\boldsymbol{\alpha}_i(y)\}$ are matrices of size $s \times s$ with entries determined by the coefficients of the operator $(\mathrm{j}\omega\mathcal{E} - \mathcal{F})$; $\{\boldsymbol{\beta}_i(y)\}$ are matrices of size $s \times r$; and $\{\boldsymbol{\gamma}_i(y)\}$ are matrices of size $p \times s$. We also normalize the coefficient of the highest derivative of each ϕ_i to one,

$$\alpha_{n_i,ii} = 1, \;\; i = 1, \ldots, s,$$

where $\alpha_{n_i,ii}$ is the iith component of the matrix $\boldsymbol{\alpha}_{n_i}$, and n_i identifies the highest derivative of ϕ_i. In order to make sure that the input field $\mathbf{d}$ in (4) does not directly influence the boundary conditions and the output field $\boldsymbol{\varphi}$, we impose the following technical assumption on system (4)

$$\ell < n, \;\; m < n - \ell, \;\; k < n - m.$$

Alternatively we can rewrite (4) into a system of first-order differential equations. This can be done by introducing state variables, $\{\mathbf{x}_i(y)\}$, where each of these states represents a linear combination of $\boldsymbol{\phi}$, $\mathbf{d}$, and their derivatives up to a certain order. Due to space limitations, we omit the detailed procedure for converting a high-order ODE with spatially varying coefficients given by (4) to a family of first-order ODEs. This transformation yields the following *spatial* state-

space representation of the frequency response operator $\mathcal{T}$

$$\mathcal{T}: \left\{ \begin{array}{rcl} \mathbf{x}'(y) & = & \mathbf{A}_0(y)\,\mathbf{x}(y) \;+\; \mathbf{B}_0(y)\,\mathbf{d}(y), \\ \boldsymbol{\varphi}(y) & = & \mathbf{C}_0(y)\,\mathbf{x}(y), \\ 0 & = & \mathbf{N}_1\,\mathbf{x}(a) \;+\; \mathbf{N}_2\,\mathbf{x}(b), \end{array} \right. \tag{5}$$

where $\mathbf{x}$ is the state vector, $\mathbf{A}_0$, $\mathbf{B}_0$, and $\mathbf{C}_0$ are matrices with, in general, spatially varying entries, and $\mathbf{N}_1$ and $\mathbf{N}_2$ are constant matrices specifying the boundary conditions. To avoid redundancy in boundary conditions, $\mathbf{N}_1$ and $\mathbf{N}_2$ are chosen such that $\left[\begin{array}{cc} \mathbf{N}_1 & \mathbf{N}_2 \end{array}\right]$ has a full row rank. We note that (5) is well-posed (that is, it has a unique solution for any input $\mathbf{d}$) if and only if $\det(\mathbf{N}_1 + \mathbf{N}_2\boldsymbol{\Phi}_0(b,a)) \neq 0$ [10], where $\boldsymbol{\Phi}_0(y,\tau)$ denotes the state transition matrix of $\mathbf{A}_0(y)$.

B. Representations of the adjoint operator $\mathcal{T}^*$

We next describe the procedure for obtaining the two point boundary value representations of the adjoint operator $\mathcal{T}^*$: $\mathbf{f} \mapsto \mathbf{g}$. As shown above, the operator $\mathcal{T}$ can be recast into the input-output differential equation (4), and the corresponding representation of $\mathcal{T}^*$ is given by

$$\mathcal{T}^*: \left\{ \begin{array}{rcl} [\,\mathcal{A}_0^*\,\boldsymbol{\psi}\,](y) & = & [\,\mathcal{C}_0^*\,\mathbf{f}\,](y), \\ \mathbf{g}(y) & = & [\,\mathcal{B}_0^*\,\boldsymbol{\psi}\,](y), \\ 0 & = & [\,\mathcal{N}_0\,\boldsymbol{\psi}\,](y). \end{array} \right. \tag{6}$$

It can be shown that

$$\begin{aligned} [\,\mathcal{A}_0^*\,\boldsymbol{\psi}\,](y) &= \sum_{i=0}^{n}(-1)^i \left[\mathbf{D}^{(i)}\,(\boldsymbol{\alpha}_i^*\,\boldsymbol{\psi})\right](y), \\ [\,\mathcal{C}_0^*\,\mathbf{f}\,](y) &= \sum_{i=0}^{k}(-1)^i \left[\mathbf{D}^{(i)}\,(\boldsymbol{\gamma}_i^*\,\mathbf{f})\right](y), \\ [\,\mathcal{B}_0^*\,\boldsymbol{\psi}\,](y) &= \sum_{i=0}^{m}(-1)^i \left[\mathbf{D}^{(i)}\,(\boldsymbol{\beta}_i^*\,\boldsymbol{\psi})\right](y). \end{aligned}$$

where $\boldsymbol{\alpha}_i^*$, $\boldsymbol{\beta}_i^*$, and $\boldsymbol{\gamma}_i^*$ are the complex-conjugate-transposes of the matrices $\boldsymbol{\alpha}_i$, $\boldsymbol{\beta}_i$, and $\boldsymbol{\gamma}_i$.

On the other hand, the state-space representation of the adjoint of the operator $\mathcal{T}$ is given by [10]

$$\mathcal{T}^*: \left\{ \begin{array}{rcl} \mathbf{z}'(y) & = & -\mathbf{A}_0^*(y)\,\mathbf{z}(y) \;-\; \mathbf{C}_0^*(y)\,\mathbf{f}(y), \\ \mathbf{g}(y) & = & \mathbf{B}_0^*(y)\,\mathbf{z}(y), \\ 0 & = & \mathbf{M}_1\,\mathbf{z}(a) \;+\; \mathbf{M}_2\,\mathbf{z}(b), \end{array} \right. \tag{7}$$

where $\mathbf{A}_0^*$, $\mathbf{B}_0^*$, and $\mathbf{C}_0^*$ denote the complex-conjugate-transposes of matrices $\mathbf{A}_0$, $\mathbf{B}_0$, and $\mathbf{C}_0$. The boundary condition matrices $\mathbf{M}_1$ and $\mathbf{M}_2$ are determined such that $\left[\begin{array}{cc} \mathbf{M}_1 & \mathbf{M}_2 \end{array}\right]$ has full row rank and

$$\left[\begin{array}{cc} \mathbf{M}_1 & \mathbf{M}_2 \end{array}\right] \left[\begin{array}{c} \mathbf{N}_1^* \\ -\mathbf{N}_2^* \end{array}\right] \;=\; 0.$$

A procedure for selecting $\mathbf{M}_1$ and $\mathbf{M}_2$ that satisfy these two requirements is given in [11]. Furthermore, we note that the well-posedness of the adjoint representation (7) is guaranteed by the well-posedness of $\mathcal{T}$.

C. Representations of $\mathcal{T}\mathcal{T}^*$

From the above described representations of $\mathcal{T}$ and $\mathcal{T}^*$, we can determine corresponding representations of $\mathcal{T}\mathcal{T}^*$: $\mathbf{f} \mapsto \boldsymbol{\varphi}$, which represents a cascade connection of the frequency response operator $\mathcal{T}$ and its adjoint $\mathcal{T}^*$. The input-output differential equation for $\mathcal{T}\mathcal{T}^*$ is obtained by equating the output of $\mathcal{T}^*$ in (6) to the input of $\mathcal{T}$ in (4), $\mathbf{d} = \mathbf{g}$, yielding

$$\mathcal{T}\mathcal{T}^*: \left\{ \begin{array}{rcl} [\,\mathcal{A}\,\boldsymbol{\xi}\,](y) & = & [\,\mathcal{B}\,\mathbf{f}\,](y), \\ \boldsymbol{\varphi}(y) & = & [\,\mathcal{C}\,\boldsymbol{\xi}\,](y), \\ 0 & = & [\,\mathcal{N}\,\boldsymbol{\xi}\,](y), \end{array} \right. \tag{8}$$

where

$$\boldsymbol{\xi}(y) = \left[\begin{array}{c} \boldsymbol{\phi}(y) \\ \boldsymbol{\psi}(y) \end{array}\right],\; \mathcal{A} = \left[\begin{array}{cc} \mathcal{A}_0 & -\mathcal{B}_0\mathcal{B}_0^* \\ 0 & \mathcal{A}_0^* \end{array}\right],$$

$$\mathcal{N} = \left[\begin{array}{cc} \mathcal{N}_0 & 0 \\ 0 & \mathcal{N}_0 \end{array}\right],\; \mathcal{B} = \left[\begin{array}{c} 0 \\ \mathcal{C}_0^* \end{array}\right],\; \mathcal{C} = \left[\begin{array}{cc} \mathcal{C}_0 & 0 \end{array}\right].$$

Similarly, the spatial state-space representation of $\mathcal{T}\mathcal{T}^*$ is obtained by setting the output $\mathbf{g}$ in (7) to be the input $\mathbf{d}$ in (5), which yields

$$\mathcal{T}\mathcal{T}^*: \left\{ \begin{array}{rcl} \mathbf{q}'(y) & = & \mathbf{A}(y)\mathbf{q}(y) \;+\; \mathbf{B}(y)\mathbf{f}(y), \\ \boldsymbol{\varphi}(y) & = & \mathbf{C}(y)\mathbf{q}(y), \\ 0 & = & \mathbf{L}_1\mathbf{q}(a) \;+\; \mathbf{L}_2\mathbf{q}(b), \end{array} \right. \tag{9}$$

where

$$\mathbf{q}(y) = \left[\begin{array}{c} \mathbf{x}(y) \\ \mathbf{z}(y) \end{array}\right],\; \mathbf{A}(y) = \left[\begin{array}{cc} \mathbf{A}_0(y) & \mathbf{B}_0(y)\mathbf{B}_0^*(y) \\ 0 & -\mathbf{A}_0^*(y) \end{array}\right],$$

$$\mathbf{L}_1 = \left[\begin{array}{cc} \mathbf{N}_1 & 0 \\ 0 & \mathbf{M}_1 \end{array}\right],\; \mathbf{L}_2 = \left[\begin{array}{cc} \mathbf{N}_2 & 0 \\ 0 & \mathbf{M}_2 \end{array}\right],$$

$$\mathbf{B}(y) = \left[\begin{array}{c} 0 \\ -\mathbf{C}_0^*(y) \end{array}\right],\; \mathbf{C}(y) = \left[\begin{array}{cc} \mathbf{C}_0(y) & 0 \end{array}\right].$$

Since a cascade connection of two well-posed systems is well-posed, the existence and uniqueness of solutions of (8) and (9) is guaranteed by the well-posedness of the corresponding two point boundary value representations of $\mathcal{T}$ and $\mathcal{T}^*$.

IV. Computation of the Maximum Singular Value of $\mathcal{T}$

In this section, we utilize structure of the above presented two point boundary value representations of $\mathcal{T}\mathcal{T}^*$ to develop a method for computing the maximum singular value of the frequency response operator $\mathcal{T}$, $\sigma_{\max}^2(\mathcal{T}) = \lambda_{\max}(\mathcal{T}\mathcal{T}^*)$. Since the operator $\mathcal{T}\mathcal{T}^*$ is positive semi-definite, all of its non-zero eigenvalues are real and positive. In view of this, we employ a power iteration scheme to determine $\lambda_{\max}(\mathcal{T}\mathcal{T}^*)$. In addition to $\lambda_{\max}$, the power iterations produce a sequence of functions that converges to the principle eigenfunction of the underlying operator.

The power iteration method requires finding the solution to

$$\boldsymbol{\varphi}(y) \;=\; [\,\mathcal{T}\mathcal{T}^*\,\mathbf{f}\,](y), \tag{10}$$

which can be obtained either by solving an input-output differential equation (8) or a system of first-ordered ODEs (9). In what follows, we present the procedure for solving (10) using both representations of $\mathcal{T}\mathcal{T}^*$. We find the solution to (8) by recasting it into a corresponding integral formulation. We then employ recently developed automatic Chebyshev spectral collocation method [3] to solve the resulting integral equation. On the other hand, the solution to (9) is

obtained using MATLAB's two point boundary value problem solver bvp4c [4].

A. Solution to a high-order differential equation using integral formulation

The solution to a two point boundary value problem (8) can be obtained numerically by approximating the differential operators using, e.g., pseudo-spectral collocation techniques. For differential equations of a high-order, the resulting finite-dimensional approximations may be poorly conditioned. This difficulty can be overcome by converting a high-order differential equation into an integral equation [12]. This conversion utilizes indefinite integration operators that are characterized by condition numbers that remain bounded upon discretization refinement. The procedure for achieving this conversion, that we present next, extends the results of [13] from a scalar case to a system of high-order differential equations. We then describe the numerical technique for solving the resulting system of integral equations.

Instead of trying to find the solution $\boldsymbol{\xi}$ to (8) directly, we introduce two unknown variables, $\mathbf{u}$ and $\mathbf{k}$. The ith component of the vector $\mathbf{u}$ is determined by

$$u_i(y) \;=\; \left[\, D^{(n_i)}\, \xi_i \,\right](y),$$

where n_i denotes the highest derivative of ξ_i in the ith equation of the system

$$[\,\mathcal{A}\boldsymbol{\xi}\,](y) \;=\; [\,\mathcal{B}\,\mathbf{f}\,](y).$$

On the other hand, $\mathbf{k}$ denotes the vector of integration constants which are to be determined from the boundary conditions. The solution $\boldsymbol{\xi}$ is then given by

$$\boldsymbol{\xi} \;=\; \mathcal{J}\,\mathbf{u} + \mathcal{K}\,\mathbf{k}, \tag{11}$$

where the operators $\mathcal{J}$ and $\mathcal{K}$ are given by

$$\mathcal{J} \;=\; \begin{bmatrix} J^{(n_1)} & & \\ & \ddots & \\ & & J^{(n_s)} \end{bmatrix},\; \mathcal{K} \;=\; \begin{bmatrix} K^{(n_1)} & & \\ & \ddots & \\ & & K^{(n_s)} \end{bmatrix},$$

with $J^{(n_i)}$ denoting the indefinite integration operator of degree n_i, and $K^{(n_i)}$ representing a matrix with columns that span the vector space of polynomials of degree less than n_i, i.e.

$$K^{(n_i)} \;=\; \begin{bmatrix} K_0(y) & K_1(y) & \cdots & K_{n_i-1}(y) \end{bmatrix},$$
$$K_0(y) \;=\; 1,\;\; K_j(y) \;=\; \frac{1}{j!}\,(y-a)^j\,.$$

Substitution of (11) into (8) yields the integral representation of the operator $\mathcal{T}\mathcal{T}^*$

$$\mathcal{T}\mathcal{T}^* : \begin{cases} \begin{bmatrix} \mathcal{A}\mathcal{J} & \mathcal{A}\mathcal{K} \\ \mathcal{N}\mathcal{J} & \mathcal{N}\mathcal{K} \end{bmatrix} \begin{bmatrix} \mathbf{u} \\ \mathbf{k} \end{bmatrix} \;=\; \begin{bmatrix} \mathcal{B} \\ 0 \end{bmatrix} \mathbf{f}, \\ \boldsymbol{\varphi} \;=\; \begin{bmatrix} \mathcal{C}\mathcal{J} & \mathcal{C}\mathcal{K} \end{bmatrix} \begin{bmatrix} \mathbf{u} \\ \mathbf{k} \end{bmatrix}. \end{cases} \tag{12}$$

Clearly, the integration constants are determined by

$$\mathbf{k} \;=\; -\,(\mathcal{N}\mathcal{K})^{-1}\,(\mathcal{N}\mathcal{J})\,\mathbf{u},$$

and invertibility of the matrix $(\mathcal{N}\mathcal{K})$ follows from well-posedness of the two-point boundary value problem (8). Finally, this expression for $\mathbf{k}$ in conjunction with (12) yields

$$\mathbf{u} \;=\; \left(\mathcal{A}\mathcal{J} - (\mathcal{A}\mathcal{K})(\mathcal{N}\mathcal{K})^{-1}(\mathcal{N}\mathcal{J})\right)^{-1}\,(\mathcal{B}\,\mathbf{f}),$$
$$\boldsymbol{\varphi} \;=\; \left(\mathcal{C}\,\mathcal{J} - (\mathcal{C}\,\mathcal{K})(\mathcal{N}\mathcal{K})^{-1}\,(\mathcal{N}\mathcal{J})\right)\,\mathbf{u}.$$

For a given $\mathbf{f}$, we can now numerically determine the solution $\boldsymbol{\varphi}$ by rewriting the input-output differential equations (8) representing $\mathcal{T}\mathcal{T}^*$ into an integral form (12). Solving the integral forms of boundary value problems is facilitated by recently developed computational package Chebfun [3]. Indefinite integration operators and functions can be easily represented in Chebfun's environment. This provides an elegant high-level language that allow users to solve the integral equations with few lines of code.

B. Solution to a spatial state-space representation

We next provide an explicit formula for the solution to the TPBVP given by a system of the first-order differential equations, and describe numerically efficient method for computing this solution.

The solution to a well-posed TPBVP (9) is given by

$$\boldsymbol{\varphi}(y) \;=\; \mathbf{C}(y)\left(\int_a^y \boldsymbol{\Phi}(y,\eta)\mathbf{B}(\eta)\mathbf{f}(\eta)\,\mathrm{d}\eta \;-\right.$$
$$\left.\boldsymbol{\Phi}(y,a)\,(\mathbf{L}_1 + \mathbf{L}_2\boldsymbol{\Phi}(b,a))^{-1}\,\mathbf{L}_2\int_a^b \boldsymbol{\Phi}(b,\eta)\mathbf{B}(\eta)\mathbf{f}(\eta)\,\mathrm{d}\eta\right),$$

where $\boldsymbol{\Phi}(y,\eta)$ denotes the state transition matrix of $\mathbf{A}(y)$. If matrix $\mathbf{A}$ is y-independent, the state-transition matrix $\boldsymbol{\Phi}(y,\eta)$ simplifies to a matrix exponential $\mathrm{e}^{\mathbf{A}(y-\eta)}$.

For a system with spatially-varying coefficients in y, a matrix-valued differential equation needs to be solved in order to obtain the state transition matrix $\boldsymbol{\Phi}(y,\eta)$ for each $y,\eta \in [a,\,b]$. For a system with constant coefficients, the matrix exponential has to be computed instead. MATLAB's initial value problem solvers, e.g., ode45 and ode15s, can be used to compute $\boldsymbol{\Phi}(y,\eta)$. We note that the computation of the state transition matrix using these solvers may be numerically ill-conditioned, thereby producing erroneous results. This problem can be circumvented by using MATLAB's two point boundary value problem solver bvp4c to directly solve (9). bvp4c explicitly accounts for the boundary conditions and it implements a Simpson's method for computing the approximate solution to, in general, nonlinear two point boundary value problems [4]. Potential numerical instabilities are avoided by dividing the integration interval $[a,\,b]$ into subintervals and by approximating the solution within each of these by a cubic polynomial.

C. An algorithm for computing the maximum singular value

We now present the standard power iteration algorithm for computing $\sigma_{\max}(\mathcal{T})$. This algorithm converges, with a geometric rate, if the initial $\mathbf{f}$ has a component in the direction of the principal eigenvector, and its rate of convergence is determined by the ratio of the second largest and the largest eigenvalues of $\mathcal{T}\mathcal{T}^*$ [14].

V. An example from viscoelastic fluid dynamics

We now use an example from viscoelastic fluid dynamics to illustrate our developments. We compute the maximum singular value using Algorithm 1 and provide comparison

Algorithm 1 Power iteration

function $[\boldsymbol{\varphi}, \lambda]$ = *power*$(\mathcal{T}\mathcal{T}^*, \mathbf{f}, tolerance)$

1: $\mathbf{f} \leftarrow \mathbf{f}/\|\mathbf{f}\|_2$; $\mathbf{f}$ satisfies the boundary conditions
2: $\mathbf{s} \leftarrow \infty$;
3: ***while*** $\|\mathbf{s}\|_2 > tolerance$ ***do***
4: $\quad\boldsymbol{\varphi}(y) \leftarrow [\mathcal{T}\mathcal{T}^*\mathbf{f}](y)$; using either the integral formulation (Section IV-A) or the state-space formulation (Section IV-B).
5: $\quad\lambda \leftarrow \|\boldsymbol{\varphi}\|_2$; $\boldsymbol{\varphi} \leftarrow \boldsymbol{\varphi}/\lambda$; $\mathbf{s} \leftarrow \mathbf{f} - \boldsymbol{\varphi}$; $\mathbf{f} \leftarrow \boldsymbol{\varphi}$;
6: ***end while***

of our results with those obtained using a standard pseudo-spectral collocation method [1].

We consider the dynamics of two-dimensional velocity and polymer stress fluctuations in an inertialess channel flow of viscoelastic fluids; see Fig. 1 for geometry. For background on the governing equations and the use of system norms in understanding the transient and asymptotic dynamics of viscoelastic fluids, we refer the reader to [15], [16]. In the absence of inertia, the dynamics of velocity and polymer stress fluctuations are governed by

$$\partial_t \boldsymbol{\tau} = \mathbf{F}_{11}\,\boldsymbol{\tau} + \mathbf{F}_{12}\,\psi \tag{13a}$$

$$\Delta^2\psi = \mathbf{F}_{21}\,\boldsymbol{\tau} + \mathbf{B}\,\mathbf{d} \tag{13b}$$

$$\begin{bmatrix} u \\ v \end{bmatrix} = \begin{bmatrix} D^{(1)} \\ -\mathrm{j}k_x \end{bmatrix}\psi \tag{13c}$$

where

$$\mathbf{F}_{11} = \begin{bmatrix} f(y) & 0 & 0 \\ WeI & f(y) & 0 \\ 0 & 2\,WeI & f(y) \end{bmatrix},$$

$$\mathbf{F}_{12} = \begin{bmatrix} 2\,We\,k_x^2 I - 2\,\mathrm{j}k_x\,D^{(1)} \\ D^{(2)} + (1+2We^2)k_x^2 I \\ 2\,\mathrm{j}k_x\,(1+2We^2)\,D^{(1)} + 2\,We\,D^{(2)} \end{bmatrix},$$

$$\mathbf{F}_{21} = \frac{(1-\beta)}{\beta}\begin{bmatrix} \mathrm{j}k_x D^{(1)} & -\left(D^{(2)} + k_x^2 I\right) & -\mathrm{j}k_x D^{(1)} \end{bmatrix},$$

$$\mathbf{B} = \frac{1}{\beta}\begin{bmatrix} -D^{(1)} & \mathrm{j}k_x I \end{bmatrix}, f(y) = -(1 + We\,\mathrm{j}k_x\,y)I,$$

$$\Delta^2 = D^{(4)} - 2k_x^2 D^{(2)} + k_x^4 I.$$

Here, $\boldsymbol{\tau} = \begin{bmatrix} \tau_{22} & \tau_{12} & \tau_{11} \end{bmatrix}^T$ with τ_{ij} denoting the polymer stress fluctuations; ψ is the stream function; and $\mathbf{d} = \begin{bmatrix} d_1 & d_2 \end{bmatrix}^T$ with d_1 and d_2 representing the body force fluctuations in the streamwise (x) and wall-normal (y) directions, respectively. The fields of interest are the streamwise (u) and the wall-normal (v) velocity fluctuations. We note that the spatial Fourier transform in x has been utilized to yield a system (13) with one spatial coordinate, $y \in [-1, 1]$, with the dynamics in x being captured by the wave-number, k_x. The important parameters that appear in the equations are the viscosity ratio, $\beta \in (0, 1)$, which is the ratio of the solvent to the total viscosity, and the Weissenberg number, We, which is the ratio of the fluid relaxation time to the characteristic flow time. It is well known that system (13) is exponentially stable for all (k_x, β, We).

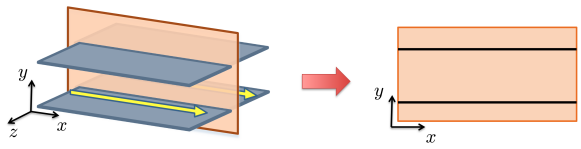

Fig. 1. Channel flow geometry. We consider the dynamics of two-dimensional flow fluctuations in the (x, y)-plane.

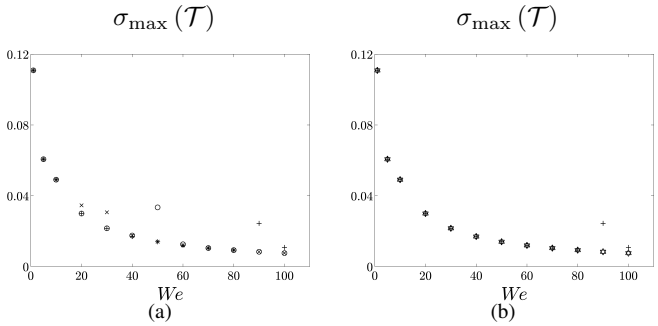

Fig. 2. Maximum singular value of the frequency response operator for an inertialess shear flow of viscoelastic fluids as a function of We at $k_x = 1$, $\beta = 0.5$, and $\omega = 0$. (a) Pseudo-spectral method (PSM) with: ×, N = 50; ○, N = 100; +, N = 200; (b) ▽, bvp4c; △, integral formulation; +, PSM with N = 200.

The polymer stresses can be eliminated from the model by substituting the temporal Fourier transform of (13a) into (13b), yielding the forced TPBVP in y for the stream function, $\psi(y)$,

$$\psi''''(y) + a_3(y)\psi'''(y) + a_2(y)\psi''(y) + a_1(y)\psi'(y) + a_0(y)\psi(y) = \begin{bmatrix} 0 & b_0(y) \end{bmatrix}\begin{bmatrix} d_1(y) \\ d_2(y) \end{bmatrix} + \begin{bmatrix} b_1(y) & 0 \end{bmatrix}\begin{bmatrix} d_1'(y) \\ d_2'(y) \end{bmatrix}. \tag{14}$$

The coefficients $\{a_i(y), b_j(y)\}$ have rather complicated expressions and are not reported here for brevity. Input-output differential equation (14) describes the frequency operator $\mathcal{T}$ and it is parameterized by ω, k_x, β, and We with the boundary conditions $\psi(y = \pm 1) = \psi'(y = \pm 1) = 0$. For notational convenience, we have suppressed the dependence of ψ, d_1, d_2, and their spatial derivatives on (ω, k_x, β, We). The ordinary differential equation representing the adjoint system can be determined using expression (6). For brevity, the state-space representation of the operator $\mathcal{T}(\omega, k_x, \beta, We)$ is not reported here.

In what follows, we fix $k_x = 1$, $\beta = 0.5$, and $\omega = 0$ and examine the effects of the Weissenberg number, We, on the frequency responses. Figure 2(a) shows the We-dependence of $\sigma_{\max}$, which is computed using a pseudo-spectral method (PSM) [1]. For $We < 10$, the maximum singular value converges as the number of collocation points, N, increases from 50 to 200. However, for $We > 10$, the increased number of collocation points in y does not necessarily produce convergent results. For example, at $We = 90$ and $We = 100$, $\sigma_{\max}$ computed using $N = 200$ is significantly larger than $\sigma_{\max}$ obtained with $N = 50$ and $N = 100$. This lack of convergence originates from the ill-conditioning of pseudo-spectral method in inertialess shear flow of viscoelastic fluids. On the other hand, the maximum singular values computed using Chebfun for the integral formulation and

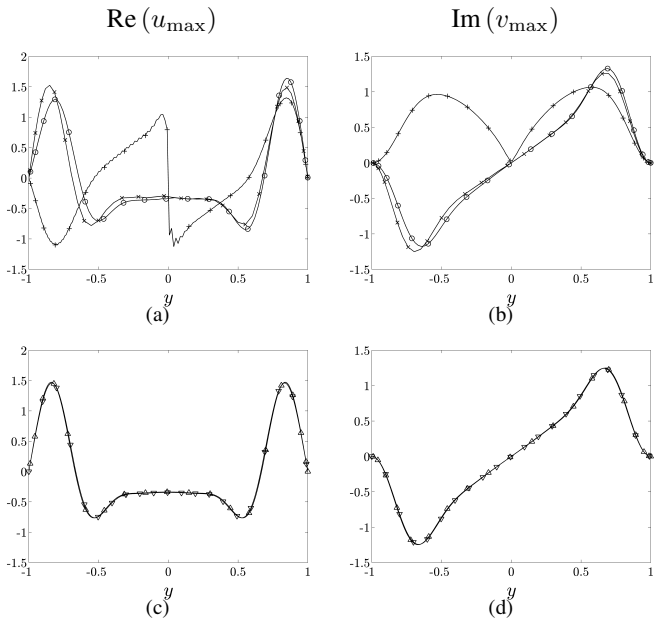

Fig. 3. Principle singular functions of the frequency response operator for inertialess shear flow of viscoelastic fluids for $We = 100$, $k_x = 1$, and $\beta = 0.5$. First row: real part of $u_{\max}$ and second row: imaginary part of v_{max}. (a) and (b) Pseudo-spectral method (PSM) with: $\times$, N = 50; $\circ$, N = 100; +, N = 200; (c) and (d) $\triangledown$, bvp4c; $\triangle$, integral formulation.

bvp4c for the spatial state-space representation are equal to each other; see Fig. 2(b) for an illustration. This figure also shows $\sigma_{\max}$ obtained using PSM with $N = 200$ collocation points in y. We note that Chebfun and bvp4c automatically adjust the number of collocation points in order to obtain solutions with an *a priori* specified tolerance.

The principal singular functions corresponding to the streamwise and wall-normal velocity fluctuations for $We = 100$ are shown in Fig. 3. Figures 3(a) and 3(b) show the same profiles obtained using a pseudo-spectral method with different numbers of collocation points. Note the lack of convergence in the profiles as the number of collocation points are increased. At $N = 200$, both the streamwise and the wall-normal profiles exhibit numerical instabilities with singularities starting to appear in the center of the channel. On the other hand, no numerical instabilities are observed with Chebfun and bvp4c, and the corresponding principal singular functions exhibit nice symmetry with respect to the center of the channel; see Figs. 3(c) and 3(d).

We end with a brief discussion about the efficiency of the power method used in conjunction with Chebfun and bvp4c for this particular example. We note that much shorter computational time was achieved by Chebfun when solving

$$\boldsymbol{\varphi}(y) \;=\; [\mathcal{T}\mathcal{T}^{*}\mathbf{f}]\,(y).$$

Furthermore, only few power iterations were required to achieve a relative error of 10^{-6} in the computation of the maximal singular value. However, depending on the initial input to the power iterations, the principal singular functions may converge very slowly. We note that this rate of convergence can be improved by employing a more advanced iterative method, e.g., Arnoldi's method. Application of the Arnoldi's method in Chebfun and bvp4c environments is a topic of our ongoing effort.

VI. Conclusion

We develop a method for computing the maximal singular value of the frequency response operator for a class of distributed system with one spatial variable. Our method avoids the need for numerical approximation of differential operators in the evolution model by recasting the frequency response operator as a two point boundary value problem. Along with recently developed state-of-the-art computational tools, Chebfun and bvp4c, our method produces results that exhibit superior accuracy compared with conventional finite-dimensional approximation schemes. We provide an example from viscoelastic fluid dynamics to illustrate the utility of our developments. Our ongoing efforts are focused on developing the efficient methods for computation of the H_∞ norm for the class of distributed systems considered in this paper.

Acknowledgments

We would like to thank Prof. Tobin A. Driscoll for useful discussions and for his help with Chebfun computing environment.

References

[1] J. A. C. Weideman and S. C. Reddy, "A MATLAB differentiation matrix suite," *ACM T. Math. Software*, vol. 26, no. 4, pp. 465–519, 2000.
[2] W. Heinrichs, "Improved condition number for spectral methods," *Math. Comp.*, vol. 53, no. 187, pp. 103–119, 1989.
[3] L. N. Trefethen, N. Hale, R. B. Platte, T. A. Driscoll, and R. Pachón, "Chebfun version 3," University of Oxford, 2009, http://www.maths.ox.ac.uk/chebfun/.
[4] J. Kierzenka and L. F. Shampine, "A BVP solver based on residual control and the Maltab PSE," *ACM T. Math. Software*, vol. 27, no. 3, pp. 299–316, 2001.
[5] R. Kupferman, "On the linear stability of plane Couette flow for an Oldroyd-B fluid and its numerical approximation," *J. Non-Newtonian Fluid Mech.*, vol. 127, no. 2-3, pp. 169–190, 2005.
[6] M. D. Graham, "Effect of axial flow on viscoelastic Taylor-Couette instability," *J. Fluid Mech.*, vol. 360, no. 1, pp. 341–374, 1998.
[7] R. F. Curtain and H. J. Zwart, *An Introduction to Infinite-Dimensional Linear Systems Theory*. New York: Springer-Verlag, 1995.
[8] R. Curtain and K. Morris, "Transfer functions of distributed parameter systems: A tutorial," *Automatica*, vol. 45, no. 5, pp. 1101–1116, 2009.
[9] K. Zhou, J. C. Doyle, and K. Glover, *Robust and Optimal Control*. New Jersey: Prentice Hall, 1996.
[10] I. Gohberg and M. A. Kaashoek, "Time varying linear systems with boundary conditions and integral operators. I. The transfer operator and its properties," *Integral Equations and Operator Theory*, vol. 7, no. 3, pp. 325–391, 1984.
[11] M. R. Jovanović and B. Bamieh, "A formula for frequency responses of distributed systems with one spatial variable," *Syst. Control Lett.*, vol. 55, no. 1, pp. 27–37, January 2006.
[12] L. Greengard, "Spectral integration and two-point boundary value problems," *SIAM J. Numer. Anal.*, vol. 28, no. 4, pp. 1071–1080, 1991.
[13] T. A. Driscoll, "Automatic spectral collocation for integral, integro-differential, and integrally reformulated differential equations," *J. Comput. Phys.*, vol. 229, pp. 5980 – 5998, 2010.
[14] G. H. Golub and C. F. Van Loan, *Matrix Computations*. Baltimore: The Johns Hopkins University Press, 1996.
[15] M. R. Jovanović and S. Kumar, "Transient growth without inertia," *Phys. Fluids*, vol. 22, no. 2, p. 023101, February 2010.
[16] M. R. Jovanović and S. Kumar, "Nonmodal amplification of stochastic disturbances in strongly elastic channel flows," *J. Non-Newtonian Fluid Mech.*, vol. 166, no. 14-15, pp. 755–778, August 2011.